scientific reports

Check for updates

OPEN

Photocatalytic activity of the biogenic mediated green synthesized CuO nanoparticles confined into MgAl LDH matrix

Hildana Tesfaye Berede[1], Dinsefa Mensur Andoshe[1], Noto Susanto Gultom[2], Dong-Hau Kuo[2], Xiaoyun Chen[3], Hairus Abdullah[2], Tadele Hunde Wondimu[1], Yi-nan Wu[4,5] & Osman Ahmed Zelekew[1]✉

The global concern over water pollution caused by organic pollutants such as methylene blue (MB) and other dyes has reached a critical level. Herein, the *Allium cepa* L. peel extract was utilized to fabricate copper oxide (CuO) nanoparticles. The CuO was combined with MgAl-layered double hydroxides (MgAl-LDHs) via a co-precipitation method with varying weight ratios of the CuO/LDHs. The composite catalysts were characterized and tested for the degradation of MB dye. The CuO/MgAl-LDH (1:2) showed the highest photocatalytic performance and achieved 99.20% MB degradation. However, only 90.03, 85.30, 71.87, and 35.53% MB dye was degraded with CuO/MgAl-LDHs (1:1), CuO/MgAl-LDHs (2:1), CuO, and MgAl-LDHs catalysts, respectively. Furthermore, a pseudo-first-order rate constant of the CuO/MgAl-LDHs (1:2) was 0.03141 min^{-1} while the rate constants for CuO and MgAl-LDHs were 0.0156 and 0.0052 min^{-1}, respectively. The results demonstrated that the composite catalysts exhibited an improved catalytic performance than the pristine CuO and MgAl-LDHs. The higher photocatalytic performances of composite catalysts may be due to the uniform distribution of CuO nanoparticles into the LDH matrix, the higher surface area, and the lower electron and hole recombination rates. Therefore, the CuO/MgAl-LDHs composite catalyst can be one of the candidates used in environmental remediation.

Currently, environmental pollution as a result of the discharging of harmful and toxic organic pollutants from different sectors such as textile, plastic, paper, leather, and other industries become a current issue and a great challenge to mankind[1]. The discharging of these toxic organic pollutants into water bodies could be a threat to aquatic life and affect human health due to their carcinogenic and mutagenic properties[2,3]. Due to these reasons, different strategies have been implemented for the removal of organic pollutants[4,5]. However, the removal of organic pollutants with conventional treatment methods is not effective due to the chemical stability, complex structure, and low biodegradability of organic pollutants[6,7]. Specially, MB is one of the most commonly used dyes which makes mankind difficult to breathe, experiences vomits, and headaches[8]. Hence, it is crucial to design effective strategies and employ advanced treatment procedures that are useful for the complete removal of organic contaminants from polluted water systems[9]. One of the strategies employed for wastewater treatment is the advanced oxidation process (AOP) with a photocatalytic degradation system[10]. For this purpose, various photocatalysts such as TiO_2[11], ZnO[12], Fe_2O_3[13], CaO[14], and CuO[15] have been investigated. Among them, CuO has been widely utilized as a photocatalyst due to its excellent photovoltaic properties, robust electro-conductivity, and low band gap[16,17].

Several physical and chemical methods have been utilized to synthesize CuO-based photocatalysts. However, most of the methods have limitations and require hazardous chemicals as a reducing agent[18,19]. To solve

[1]Department of Materials Science and Engineering, Adama Science and Technology University, Adama, Ethiopia. [2]Department of Materials Science and Engineering, National Taiwan University of Science and Technology, Taipei 10607, Taiwan. [3]College of Materials Engineering, Fujian Agriculture and Forestry University, Fuzhou 350002, China. [4]College of Environmental Science and Engineering, State Key Laboratory of Pollution Control and Resource Reuse, Tongji University, 1239 Siping Rd., Shanghai 200092, China. [5]Shanghai Institute of Pollution Control and Ecological Security, 1239 Siping Rd., Shanghai 200092, China. ✉email: osman.ahmed@astu.edu.et; osmax2007@gmail.com

the limitations, a greener, cheaper, environmentally-friendly, simple, and non-toxic biological route has been applied to fabricate CuO NPs. In addition to this, using plant extracts in the synthesis of nanoparticles is considered as a potential candidate due to simplicity, large-scale production, and easy handling owing to natural reducing and capping agents[20]. For this purpose, several studies have been reported in the fabrication of CuO using biogenic-mediated strategies such as *Solanum lycopersicum*[21], *Solanum nigrum*[8], and *Psidium guajava*[22]. However, the biosynthesis of CuO NPs using the *Allium cepa* L. peel extract combined with LDHs has not been reported. Based on the above considerations, utilization of the *Allium cepa L* peel extracts in the preparation of nanoparticles is useful since it contains high concentrations of flavonoids and polyphenol compounds which are used as natural reducing and capping agents[23].

Although CuO is a preferable semiconductor in photocatalytic applications, its activity is limited due to the higher electron and hole pairs recombination rates[24]. To improve the photogenerated electron and hole pairs separation efficiencies, different strategies such as doping[25], heterojunction formation[26], or combined with supports[27], etc. have been implemented. Among the strategies, using support in the fabrication of catalysts showed higher catalytic performance than unsupported catalysts due to the interaction of organic pollutants on the surface of support via adsorption and reduction in electron–hole recombination rates[28]. Due to these reasons, the research works with different supports such as graphene oxide[29], carbon nanotubes[30], and layered double hydroxides (LDHs)[31] have been reported.

LDHs are hydrotalcite-like and inorganic layered substances made up of positively charged brucite-like host layers and charge-balancing interlayer anions. Their large surface areas make them ideal catalysts or precursors[32]. The LDHs are commonly employed in catalysis, adsorption, electrochemistry, and biotechnology as typical two-dimensional-nano structured anionic clays[33]. Apart from the multiple positive charges on the LDHs platelets, the heterojunction interface has enough interlayer water molecules and hydroxide ions to form ·OH. The layer structure, in particular, may improve the effectiveness of photocatalytic processes by encouraging electron transport, inhibiting electron and hole recombination rates, and preventing nanoparticle aggregations[34]. Due to their superior properties, LDHs were deemed an appropriate substrate for growing nanoparticles to achieve synergistic effects and improved properties. Among them, the binary layered double hydroxides with magnesium and aluminum in the laminate have been widely used in photocatalysis[35]. However, the MgAl-LDH alone has limited photocatalytic activity under visible light irradiation. For these reasons, different composites such as TiO_2/MgAl-LDH[36], SnO_2/MgAl-LDH[37], and CeO_2/MgAl-LDH[38] have been reported.

Herein, a green approach using *Allium cepa* L. peel extract has been applied for the synthesis of CuO NPs and confined into the MgAl-LDH matrix for photocatalytic applications. The LDH layered structure could be used for effective electron migrations and electron–hole pair recombination rate suppression. The large number of hydroxyl groups on LDH laminates can also generate ·OH species, which is useful for boosting the photocatalytic activity and quantum efficiency[39]. Moreover, the green synthesized CuO nanoparticles could be also effective due to the wider visible light absorption ranges. It is expected that the composite catalysts could have improved performance than the single components due to the uniform dispersion of CuO NPs, high adsorption capacity of LDH, higher surface area, and lower electron and hole recombination rates.

Experimental

Chemicals

All chemicals and reagents were analytic grades and used without further purifications. Copper nitrate trihydrate ($Cu(NO_3)\cdot 3H_2O$, 95%), magnesium chloride hexahydrate ($MgCl_2\cdot 6H_2O$, 99%), aluminum nitrate nonahydrate ($Al(NO_3)_3\cdot 9H_2O$, 98%), sodium bicarbonate ($NaHCO_3$, 99.5%), sodium hydroxide (NaOH, 98%), ethanol (CH_3CH_2OH, 99.5%), hydrochloric acid (HCl, 37%), ethylenediamine tetra-acetic acid disodium salt (EDTA-2Na), isopropanol (IPA), and silver nitrate ($AgNO_3$) were used. The fresh onion peels (*Allium cepa* L.) were collected from a cafeteria of Adama Science and Technology University. DI water was used throughout the experiment.

Preparation of plant extract

The *Allium cepa* L. peel plant extraction process was performed according to literature report with modification[40]. In a particular procedure, the *Allium cepa* L. peels were washed with distilled water several times before being dried at 85 °C. The dried *Allium cepa* L. peels were then cut into small pieces. Then, five grams of the peel was transferred to a flask and 350 mL of distilled water was added. The mixture was stirred and boiled at 70 °C for 30 min to get an aqueous extract. Then, the solution was cooled at room temperature and filtered through filter paper.

Synthesis of CuO nanoparticles (CuO NPs)

In the preparation of CuO NPs, copper nitrate trihydrate ($Cu(NO_3)\cdot 3H_2O$), sodium hydroxide (NaOH), and *Allium cepa* L. peel extract were used based on the literature report with minor modifications[22]. Specifically, 1.208 g of $Cu(NO_3)_2\cdot 3H_2O$ was dissolved into 100 mL of distilled water. Then, the resulting solution was dropped into an aqueous extract of *Allium cepa* L. peel (100 mL) under stirring for 45 min at room temperature. Then, aqueous solution of NaOH (0.5 mol L^{-1}) was added to attain a pH of 10. The entire reaction was carried out at 70 °C for 3 h with constant stirring. The solution was aged for 24 h before being centrifuged and dried overnight at 80 °C. Finally, the powder sample was calcined at 400 °C for 2 h.

Preparation of MgAl-LDHs

The MgAl-LDHs preparations were carried out using a co-precipitation method with Mg^{2+}/Al^{3+} molar ratio of 3:1 according to a literature report with modification[41]. Briefly, an aqueous solution containing NaOH (4 g)

and $NaHCO_3$ (6.30 g) was added drop-wise to 100 mL of salt solution containing $MgCl_2{\cdot}6H_2O$ (0.015 mol) and $Al(NO_3)_3{\cdot}9H_2O$ (0.005 mol) and stirred at 60 °C in water bath. The pH was set to 10.5 and the reaction was performed under continuous stirring for 2 h. The resulting precipitate was extensively rinsed with deionized water until the pH was neutral, after being aged at 60 °C for 12 h. The solid residue was collected and dried at 80 °C for 12 h.

Preparation of CuO/MgAl LDHs nanocomposites

Co-precipitation was used to prepare the CuO/MgAl-LDHs (1:2) composite catalyst. To obtain a uniform suspension, the prepared CuO (0.3077 g) was ultrasonically dispersed in 100 mL distilled water for 1 h and then placed in a 60 °C water bath with stirring. Then, a salt solution containing 0.192 g $MgCl_2{\cdot}6H_2O$ and 0.2424 g $Al(NO_3)_3{\cdot}9H_2O$ were added to the suspension. To keep the pH at 10.5, an aqueous solution containing NaOH (4 g) and $NaHCO_3$ (6.30 g) was added drop-wise. The precipitate was aged at 60 °C for 12 h and then washed with deionized water until the solution became neutral. Finally, the composite was dried for 12 h at 80 °C[42]. For comparison purposes, different weight ratios of the CuO/LDHs abbreviated as CuO/MgAl-LDHs (1:2), CuO/MgAl-LDHs (1:1), and CuO/MgAl-LDHs (2:1) were prepared. The preparation of the composite catalyst is shown in Scheme 1.

Photocatalytic activity

The photocatalytic activities of the catalysts were checked by the degradation of MB dye. In the degradation process, 25 mg of the catalyst was added into 100 mL (10 mg L^{-1}) of MB dye solution and stirred for 30 min to establish an adsorption–desorption equilibrium in the dark. Then, the suspension was exposed to a 150 W halogen lamp for 80 min under regular stirring. To analyze the degradation of the dye, 5 mL of the aliquot was taken every 20 min of reaction time followed by centrifugation. The absorbance at a maximum wavelength of 664 nm was used to determine the concentration of the dye leftover. The radicals scavengers effects in the degradation process of MB dye were performed and EDTA-2Na, isopropyl alcohol, and $AgNO_3$ were used for trapping of h^+, ·OH, and e^-, respectively[43,44]. The stability of the CuO/MgAl-LDHs (1:2) catalyst was also checked according to the literature report with modification[45]. After each cycle, the catalyst was recovered by centrifugation, washed with deionized water, and dried in an oven at 80 °C.

Characterizations

X-ray diffractometer (Shimadzu XRD-7000) with Cu Kα radiation (λ = 1.5406 Å) operating in the range of 2θ = 10° to 80, 30.0 mA applied current, and 40.0 kV acceleration voltage was used to check the crystallinity and phases of the samples. The average crystallite size (D) and interplanar spacing (d) were calculated according to Debye–Scherrer equation and Bragg's Law, respectively[46,47]. Fourier transforms infrared spectroscopy (FTIR-6600 type A) was used to check bonding and functional groups of the samples in the range 4000–400 cm^{-1}. The morphologies of the samples were examined by field-emission scanning electron microscopy (FE-SEM, JSM 6500F, JEOL) and transmission electron microscopy (TEM) (FEG TEM Tecnai G2 F30). X-ray photoelectron spectroscopy (XPS) (ESCALAB 250) was used to examine the chemical states of the sample. The JASCD FB-8500 photoluminescence (PL) spectroscopy was used to check the electron and hole separation rates. A Shimadzu-3600 plus UV–vis spectrophotometer was used to analyze the concentration of MB dye at a maximum wavelength of 664 nm. JASCD V-670 UV–visible–near-infrared (UV–vis–NIR) spectrophotometer was used to measure UV–vis diffuse reflectance spectra (DRS) using $BaSO_4$ as a reference.

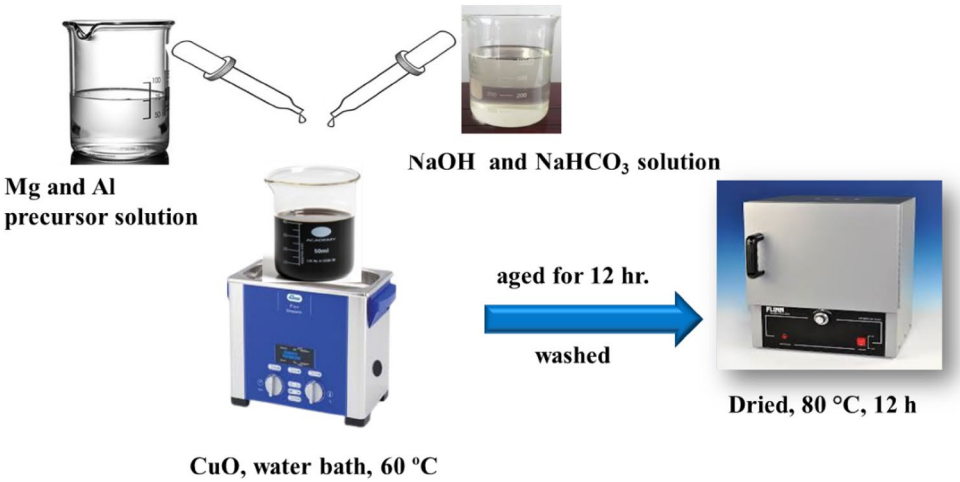

Scheme 1. Schematic diagram for the synthesis of CuO/MgAl-LDHs composite catalyst.

Results and discussion

Characterizations

The XRD patterns of the CuO NPs, MgAl-LDHs, and CuO/MgAl-LDHs composites with different weight ratios such as CuO/MgAl-LDHs (1:2), CuO/MgAl-LDHs (1:1), and CuO/MgAl-LDHs (2:1) are shown in Fig. 1. The characteristic peaks at 32.42°, 35.47°, 38.68°, 48.76°, 53.43°, 58.16°, 61.51°, 66.07°, 67.89°, 72.29°, and 75.00° correspond to the crystal planes of (110), ($\bar{1}$11), (111), (20$\bar{2}$), (020), (202), (11$\bar{3}$), (31$\bar{1}$), (113), (311), and (004), respectively, for CuO (Fig. 1a). The existence of all peaks correspond to the monoclinic CuO phase which is consistent with the reported research (JCPDS No. 00-048-1548)[48]. Moreover, the average crystallite size for CuO was also calculated and showed 16.1 nm with an interplanar spacing of 0.23 nm. Furthermore, as shown in Fig. 1b, the MgAl-LDHs peaks at 2θ of 11.4° and 23.0°, respectively, are matched with (003) and (006) crystal planes of $Mg_6Al_2(OH)_{18}{\cdot}4.5H_2O$ (JCPDS No. 22-0700). The phases are attributed to the hydrotalcite-type materials in a hexagonal lattice with R-3m rhombohedral symmetry which confirms the successful preparation of LDHs[49]. The major peaks at 2θ values of 11.44°, 23.03°, 34.75°, 39.06°, 46.41°, 60.54°, and 61.78° correspond to the crystal planes of (003), (006), (009), (012), (018), (110), and (113), respectively[50]. The average crystallite size for MgAl-LDHs was 7.95 nm with the interparticle spacing 0.39 nm. Moreover, the CuO/MgAl-LDHs XRD peaks clearly displayed the distinct peaks corresponding to both the CuO NPs and MgAl-LDHs. The results indicated that successful incorporation of CuO into LDHs was achieved. However, the prominent peaks observed confirmed the predominance of CuO in the sample. The presence of MgAl-LDHs as a carrier did not affect the structure of CuO NPs, as shown in Fig. 2c–e[39]. The average crystallite sizes were also calculated and showed 15.35, 13.9, and 12.5 nm for CuO/MgAl-LDHs (1:1), CuO/MgAl-LDHs (2:1), and CuO/MgAl-LDHs (1:2) samples, respectively. The results demonstrated that successful incorporation of CuO into LDHs was achieved.

The XPS analysis was used to investigate the chemical states of the elements in the CuO/MgAl-LDHs (1:2) composite sample. The peaks located at 933.8 and 953.8 eV, correspond to Cu $2p_{3/2}$ and Cu $2p_{1/2}$, respectively, which indicates the presence of Cu^{2+} in the CuO (Fig. 2a). Furthermore, the broad satellite peaks at a higher binding energy provided additional confirmation of the CuO. The Cu 2p was accompanied by two satellite peaks on the higher binding energy side at 943.8 eV and 941.5 eV, indicating the presence of CuO[51]. Moreover, the satellite peak at around 943.8 eV clearly demonstrates an open $3d^9$ shell, thus, supporting the presence of Cu^{2+} in the sample, which is positioned at higher binding energies than the main peaks[52,53]. Moreover, the high-resolution spectrum of the Mg 2p is also presented in Fig. 2b. In the Mg 2p spectra, a single peak appears at 49.6 eV, corresponding to Mg^{2+} in the brucite layers of MgAl-LDHs[54]. The Al 2p spectrum, deconvoluted into two peaks at 75.15 and 77.15 eV, can be assigned to Al 2p (α) and Al 2p (β) of $Al(OH)_3$ and Al_2O_3, respectively, emerging from the LDHs structure, as shown in Fig. 2c[55]. Similarly, the binding energy at 529.4 eV belongs to lattice oxygen in the O 1s spectrum, while the peak at 531.6 eV reflects chemisorbed oxygen and coordinated lattice oxygen (Fig. 2d)[56].

The FE-SEM was used to evaluate the morphological properties of the CuO NPs, MgAl-LDHs, and CuO/MgAl-LDHs (1:2) samples as shown in Fig. 3a–c. As it was observed in Fig. 3a, the CuO NPs had a spherical-like morphology. The biogenic-mediated preparation makes the CuO nanoparticles smaller and spherical morphology with different sizes. The smaller particles agglomerate and organize themselves into larger spheres[57]. In the preparation, the presence of functional groups in the plant extract encourages dynamic behavior during nucleation and stabilization[58]. Figure 3b displays the sheet-like structure of the prepared MgAl-LDHs. Moreover, Fig. 3c, showed the SEM image of the CuO/MgAl-LDHs (1:2) sample. The image reveals the uniform and dense distribution of CuO NPs in the MgAl-LDHs. The elemental composition of the as-synthesized catalyst was also

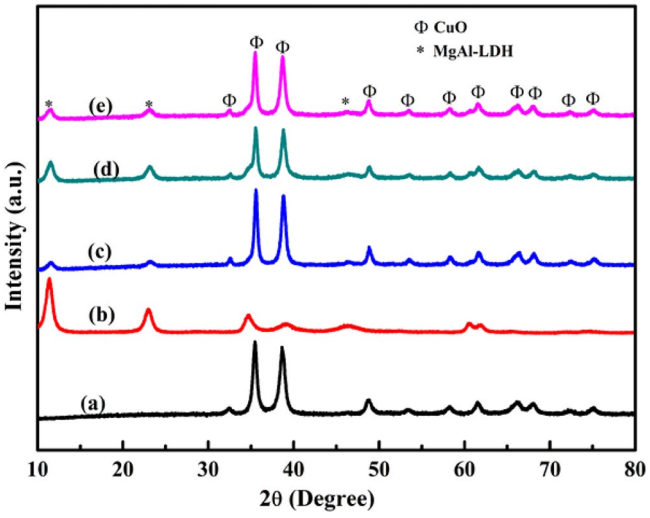

Figure 1. XRD patterns for: (**a**) CuO NPs, (**b**) MgAl-LDHs, (**c**) CuO/MgAl-LDHs (2:1), (**d**) CuO/MgAl-LDHs (1:2), and (**e**) CuO/MgAl-LDHs (1:1).

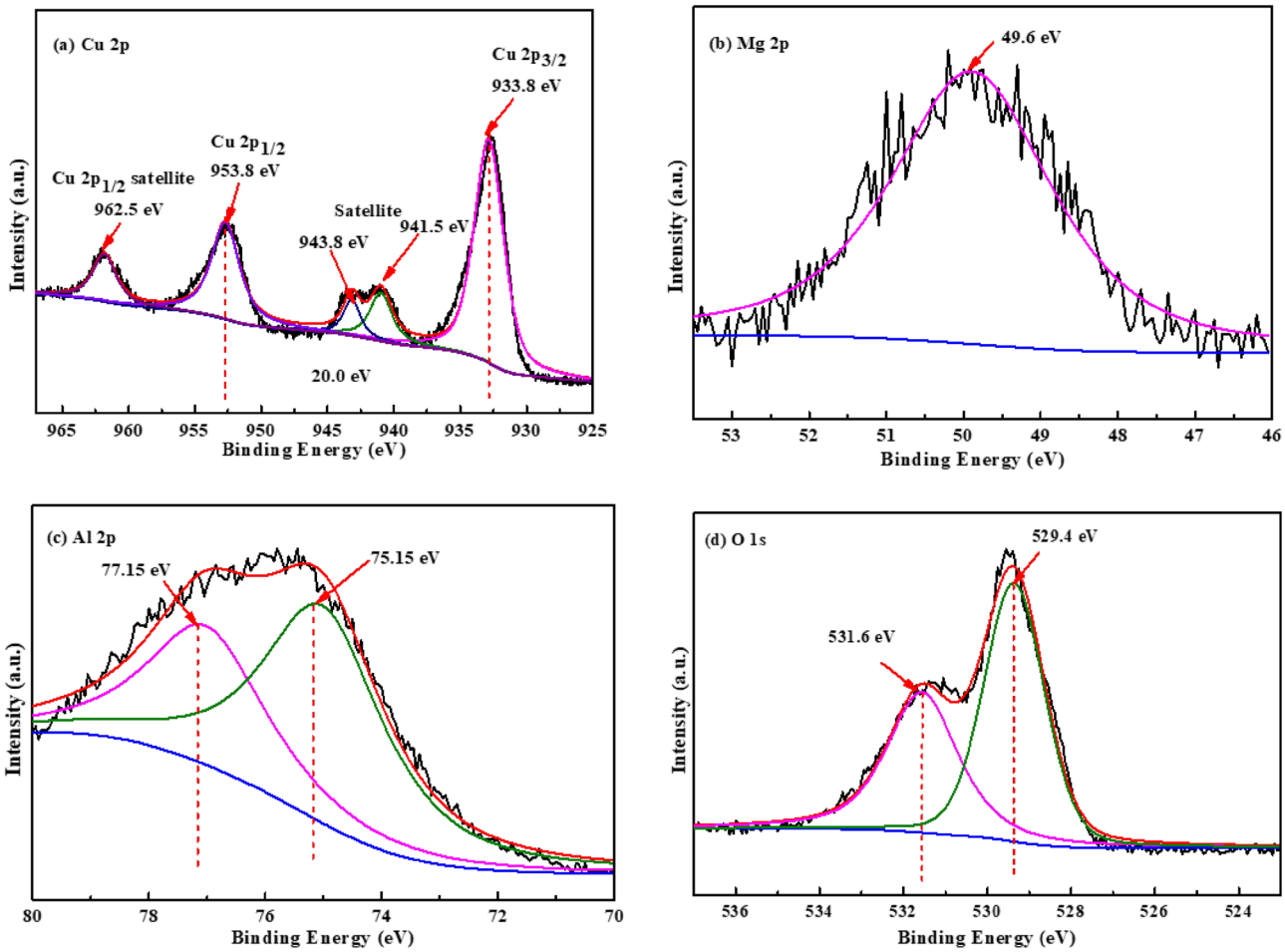

Figure 2. XPS spectra of (**a**) Cu 2p, (**b**) Mg 2p, (**c**) Al 2p, and (**d**) O 1s for CuO/MgAl-LDHs (1:2) sample.

analyzed through the EDS analysis (Fig. 3d). The EDS spectrum of CuO/MgAl-LDHs (1:2) revealed the presence of Mg, Al, O, and Cu elements.

To understand the morphology and microstructure of the sample in detail, the TEM analysis was performed. The TEM and HRTEM of the CuO/MgAl-LDHs (1:2) nanocomposite are indicated in Fig. 4. TEM image confirms that dark spots of CuO nanoparticles are distributed in the matrix of LDHs (Fig. 4a). Moreover, the d-spacing of the particles adhered to the surface of the LDH support is 0.234 nm, as shown from the HRTEM image (Fig. 4b), which belongs to the CuO (111) plane. The results revealed that the composites of the nanosized CuO-LDHs matrix were formed. Zeta potential (ZP) measurements were also performed to check the stability of the particles suspensions and their surface charge properties[59]. The average zeta-potential values for CuO, MgAl-LDHs, and CuO/MgAl-LDHs (1:2) catalysts were + 15.45 mV, + 32.7 mV, and + 19.75 mV, respectively, and shown in Fig. 1S (Supplementary). The lower dispersions ZP values will a tendency of coagulation, aggregation, or flocculation due to van der Waals interparticle attraction[60]. After CuO was incorporated into LDHs, the dispersion of ZP f was changed to + 19.75 mV, indicating that the CuO particles were well dispersed into MgAl-LDHs matrix which is also confirmed TEM analysis (Fig. 4).

The functional groups of the as-prepared CuO NPs, MgAl-LDHs, and CuO/MgAl LDHs (1:2) samples were investigated by FTIR spectroscopy. As shown in Fig. 5a,b, the O–H stretching vibrations were represented by an absorption band at 3427 cm^{-1}. An asymmetric stretching of C–O occurs at 1244 cm^{-1} resulting in cyclic polyphenol compounds[61]. In Fig. 5c, the stretching modes of the O–H groups associated with metal cation bonds in the hydroxide layer and the stretching vibrations of interlayer water molecules, attributed to the strong and broad absorption peak at 3440 cm^{-1} for pure MgAl-LDHs[42]. The asymmetric vibration of CO_3^{2-} anions and the bending vibration of water molecules between layers in the interlayer region affected the peaks at 1345 cm^{-1} and 1622 cm^{-1}, respectively, while the presence of C–O and C=O bonds might cause the CO_3^{2-} peak to break[35,62]. The vibrations of M–O/M–O–M (M = Mg, Al) characteristic of the double-lamellar structure are responsible for the remaining bands below[63] 1000 cm^{-1}. The CuO/MgAl-LDHs (1:2) spectrums comprised all feature bands of CuO NPs and MgAl-LDHs, as shown in Fig. 5d.

The optical properties of the CuO NPs, MgAl-LDHs, and CuO/MgAl-LDHs (1:2) samples were examined and shown in Fig. 6a. The absorbance of the MgAl-LDHs was lower than that of CuO and CuO/MgAl-LDHs (1:2). However, the absorbances of the CuO NPs and CuO/MgAl-LDHs samples were higher as compared to bare MgAl-LDHs. The results indicated that the enhanced absorption of the CuO/MgAl-LDHs composite

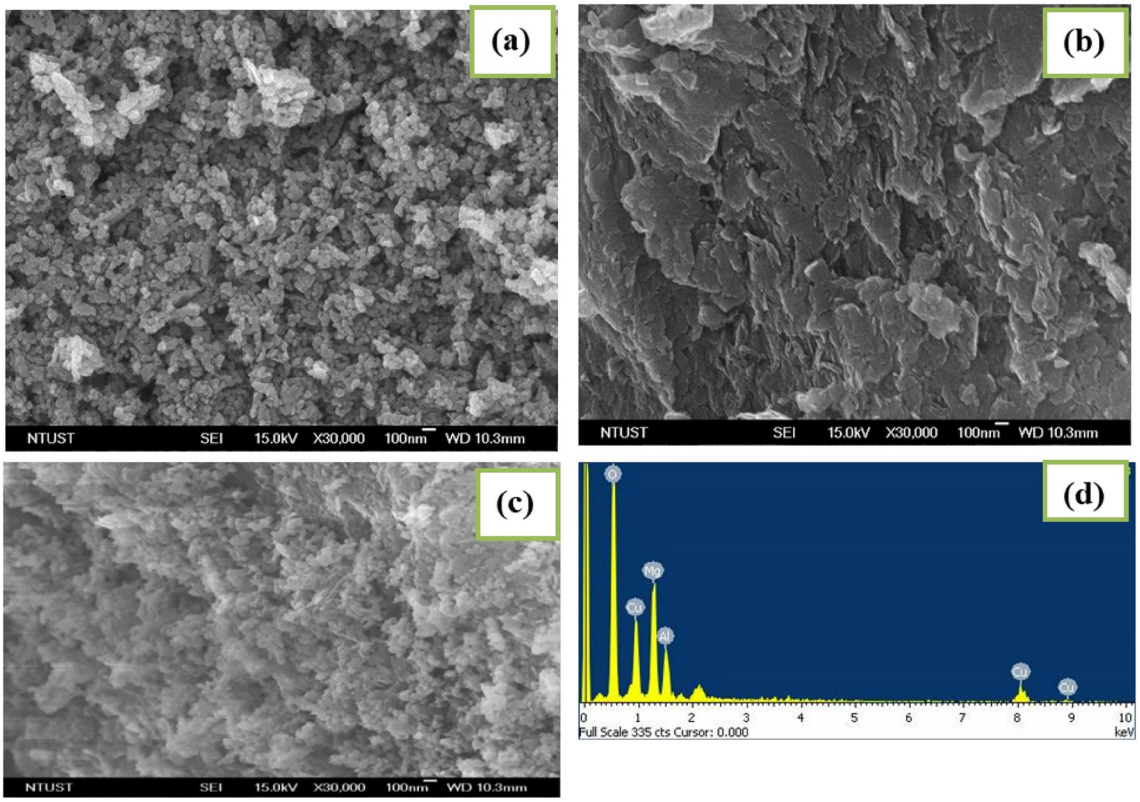

Figure 3. SEM images of: (**a**) CuO NPs, (**b**) MgAl-LDHs, and (**c**) CuO/MgAl-LDHs (1:2), and (**d**) EDS spectra for CuO/MgAl-LDHs (1:2) samples.

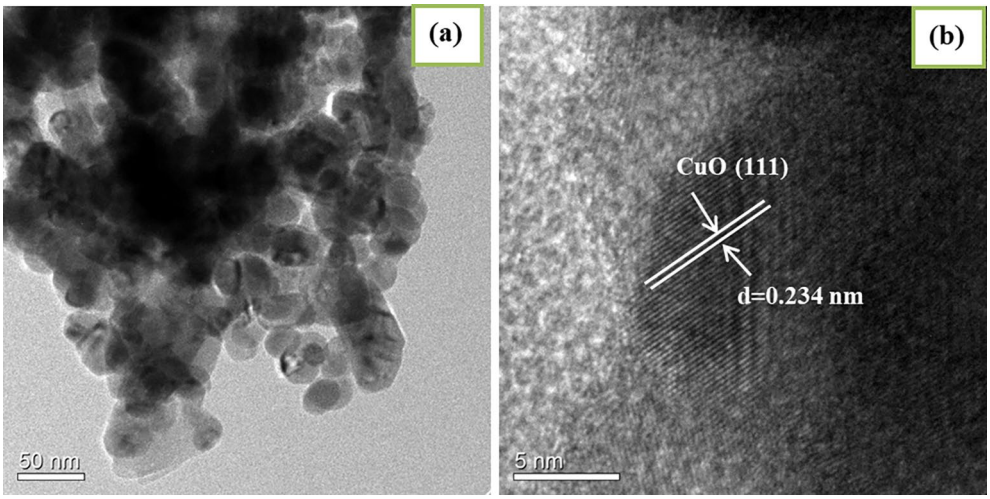

Figure 4. (**a**) TEM, and (**b**) HRTEM images of CuO/MgAl LDHs (1:2) nanocomposites.

sample could be due to the visible light- responsive property of CuO. Although CuO had higher absorbance in the visible light region, the photocatalytic performance could be lower due to the higher electron and hole recombination rates. However, significant adsorption intensity enhancement of the MgAl-LDHs may be attributed to the quantum effect of CuO which will inhibit the electron–hole pair's recombination rate that facilitates the degradation efficiency.

The PL emission spectra of CuO NPs, MgAl-LDHs, and CuO/MgAl-LDHs (1:2) composite were performed at 300 nm exited energy and are shown in Fig. 6b. The PL emission peak for the CuO/MgAl-LDHs (1:2) is substantially reduced, indicating a higher separation efficiency of photoinduced charge carriers than bare samples[54]. The rate of the recombination of excited electron–hole pairs determines the intensity of PL emission. The higher intensity indicates a faster recombination rate, while the lower intensity indicates a large amount of transferred

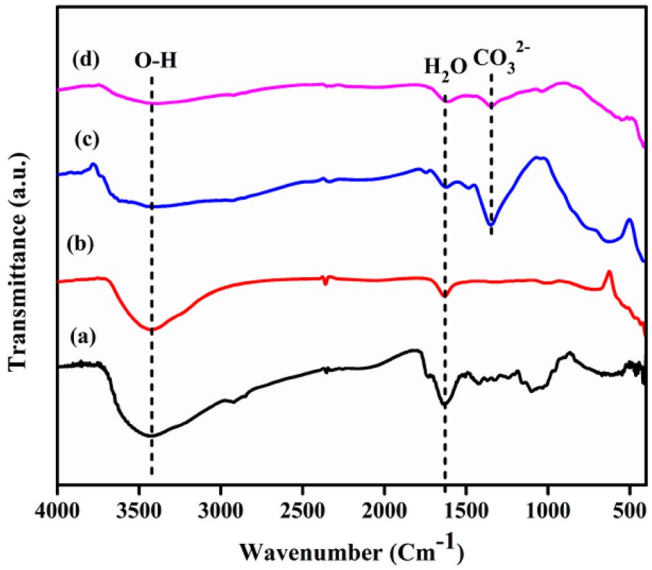

Figure 5. FTIR spectra of: (**a**) *Allium cepa* L. peels extract, (**b**) CuO NPs, (**c**) MgAl-LDHs, and (**d**) CuO/MgAl-LDHs (1:2).

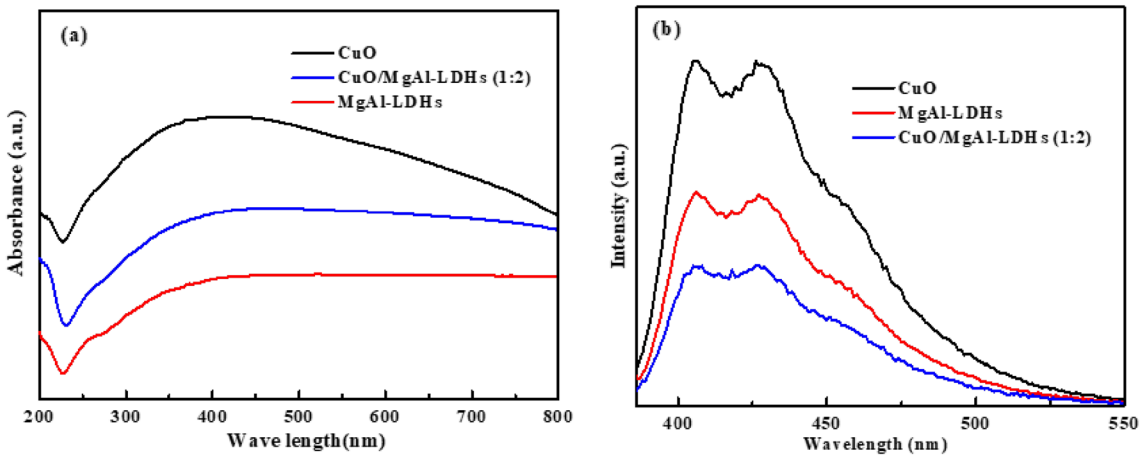

Figure 6. (**a**) UV–vis absorption and (**b**) PL spectra of CuO NPs, MgAl-LDHs, and CuO/MgAl-LDHs (1:2).

or trapped electrons in which the recombination rate is suppressed. The CuO/MgAl-LDHs (1:2) composite had much lower emission intensity than CuO NPs and MgAl-LDHs bare samples indicating that the recombination of the photogenerated electron–hole pairs was effectively inhibited. The inhibition of the electron–hole pairs facilitates the degradation of organic pollutants[64].

Photocatalytic activities

The photocatalytic performances of the CuO NPs, MgAl-LDHs, CuO/MgAl-LDHs (1:1), CuO/MgAl-LDHs (1:2), and CuO/MgAl-LDHs (2:1) composite samples were tested in the degradation of MB dye. The UV–vis absorption spectra for the MB degradations are shown in Fig. 7. As demonstrated in Fig. 7a–e, the time-dependent dye absorption intensity was decreased after the photocatalytic reaction was performed. The higher photocatalytic performance was observed in the presence of CuO/MgAl-LDHs (1:2) sample than other samples within 80 min irradiation time. The results also indicated that the addition of the optimum amounts of CuO in the composite preparation system can affect the photocatalytic properties. It can be also demonstrated that the composite catalyst showed better performances than bare CuO NPs and MgAl-LDHs samples. It could be due to interfacial charge transfers which facilitate the electron migration and suppression of electron and hole recombination[41].

Moreover, the degradation performance was also demonstrated as shown in Fig. 8a. The degradation of MB was almost negligible throughout the catalyst (blank). The photodegradation efficiency of MB with CuO/MgAl-LDHs (1:2) was 99.20%. However, the MgAl-LDHs, CuO NPs, CuO/MgAl-LDHs (2:1), and CuO/MgAl-LDHs (1:1) catalyst degradation efficiencies were 35.53, 71.87, 85.30, and 90.03%, respectively. Furthermore, the MgAl-LDHs demonstrated high adsorption of MB molecules in the dark. It can be attributed to MgAl LDHs

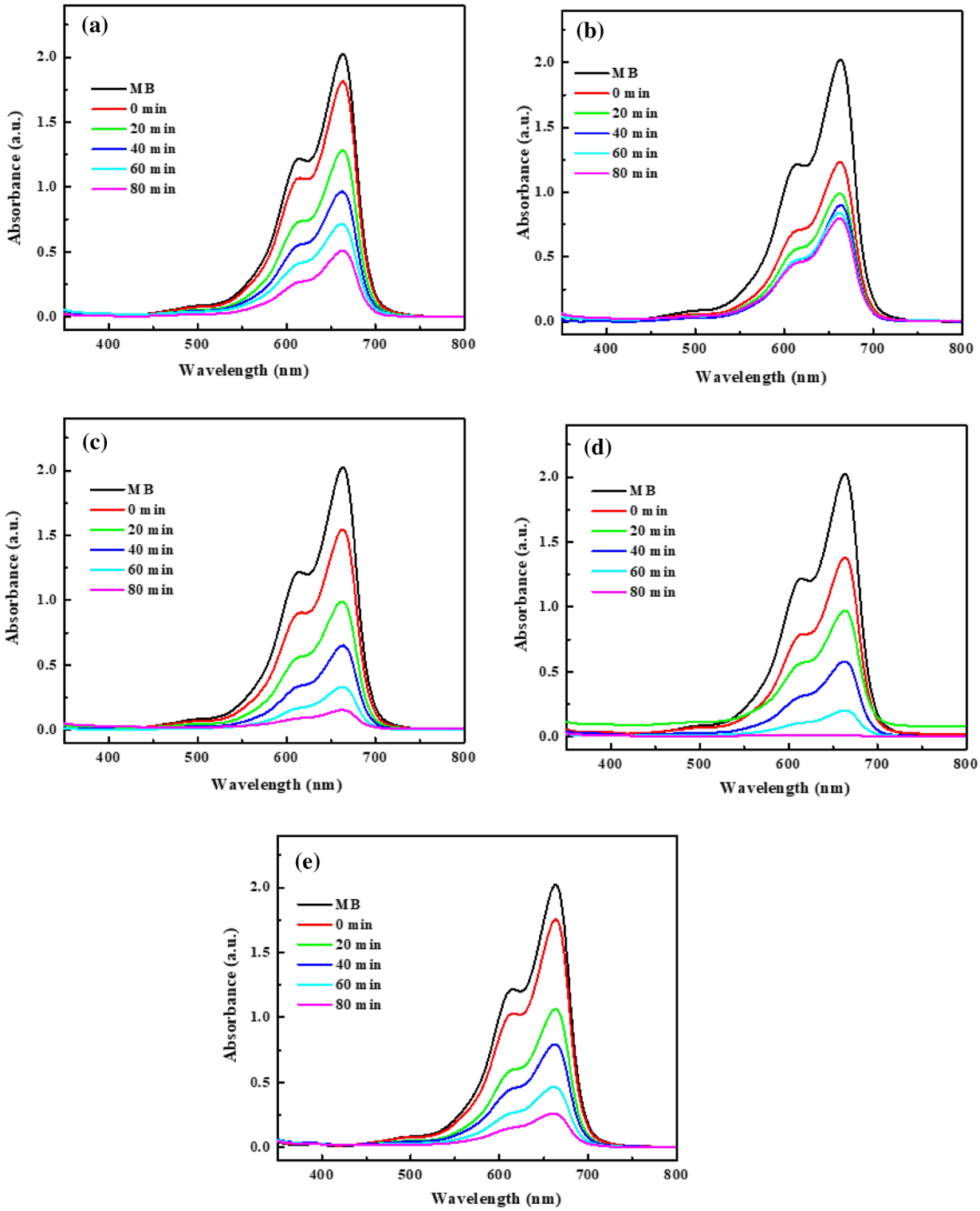

Figure 7. UV–vis absorption spectra for MB degradation with (**a**) CuO NPs, (**b**) MgAl-LDHs, (**c**) CuO/MgAl-LDHs (1:1), (**d**) CuO/MgAl-LDHs (1:2), and (**e**) CuO/MgAl-LDHs (2:1).

having a large surface area and low visible light activity. Zhou et al. discovered similar results of MgAl-LDHs[65]. The findings suggest that CuO are critical for photocatalytic activity, and adding CuO NPs into MgAl-LDHs could boost photocatalytic activity.

Figure 8b,c provides detailed information on the kinetic parameters of pseudo-first-order fitting for MB degradation[66]. The degradation rate constant (k) for CuO/MgAl-LDHs (1:2) was estimated to be 0.0314 min^{-1}, while the kinetic rates for CuO, LDHs, CuO/MgAl-LDHs (2:1), and CuO/MgAl-LDHs (1:1) samples were 0.0156, 0.0052, 0.0234, and 0.02855 min^{-1}, respectively. The CuO/MgAl-LDHs (1:2) kinetic value was higher than that

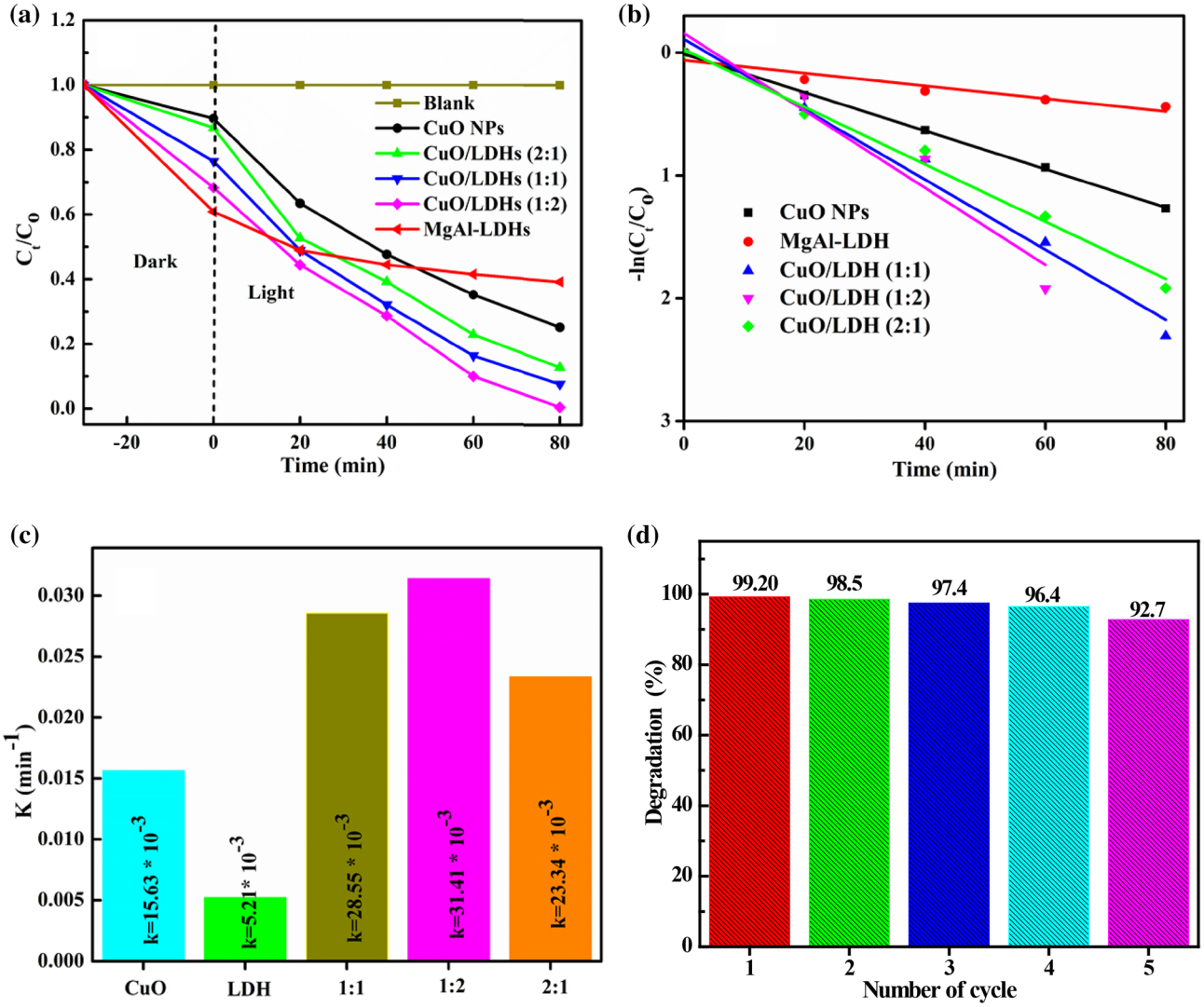

Figure 8. (**a**) The C/C_0 versus irradiation time plot of the MB degradation with different catalysts, (**b**,**c**) the kinetics study of different catalysts, and (**d**) the stability of CuO/MgAl-LDHs (1:2) sample.

of all other samples. The findings showed that the CuO/MgAl-LDHs (1:2) composite had the best photocatalytic activity in visible light irradiation. Moreover, the catalytic performance of the composite catalyst was also compared with other literature reports. As it is demonstrated in Table S1 (Supplementary), the CuO/MgAl-LDHs (1:2) composite catalyst was comparable with other catalysts in the degradation of organic pollutants. Figure 8d also demonstrates the stability of the CuO/MgAl-LDHs (1:2) composite catalyst. The CuO/MgAl-LDHs (1:2) composite catalyst showed higher photocatalytic stability after five cycles. The slightly reduced activity was primarily due to the mass loss of the photocatalyst during centrifugation to collect the reused catalyst. After five cycles, 92.7% of the MB dye degradation was maintained.

The photocatalytic degradation mechanism was proposed according to the experimental findings and characterizations results. When the photon energy which is equal to or greater than the band gap energy strikes the surface of the CuO/MgAl-LDHs, the electrons will be ejected from the balance band and moved to the conduction band[67]. The CuO creates electron–hole pairs and the positive charges on the surface of LDHs platelets can attract electrons (e^-) produced by the CuO particles, while the holes (h^+) move to the opposite direction, leading to the separation of the photogenerated e^- and h^+ pairs[34]. The photogenerated holes (h^+) reacted with hydroxyl ions to produce hydroxyl radicals (·OH), and the ·OH radicals will oxidize the organic contaminants[68]. Furthermore, the LDH layer's surface $^-$OH groups reacted with valence band holes to produce hydroxyl radicals (·OH), which are significant variables in photo-oxidation reactions[39]. Similarly, the holes can directly interact with organic pollutants and degradation will be facilitated. According to the experimental finding of scavenging effects (Fig. S2) (Supplementary), the degradation efficiency in the presence of isopropanol (·OH scavenger) significantly decreased. However, in the presence of EDTA-2Na (h^+ scavenger) and $AgNO_3$ (e^- scavenger), the degradation efficiencies were better than in the presence isopropanol. As it was demonstrated from trapping experiments, the catalyst performance without scavengers was much higher than that of the degradation in the presence of scavengers. Simultaneously, superoxide radicals ($^{\cdot}O_2^-$) were formed when excited electrons were interacted by dissolved oxygen species in an aqueous solution[67]. Organic matter could be decomposed into CO_2

and H_2O after interaction with reactive h^+, $\cdot O_2^-$ and ·OH species[69]. Therefore, the ·OH, $\cdot O_2^-$, h^+, e^- reactive species can be responsible for the degradation of MB dye using CuO/MgAl-LDHs nanocomposites. Moreover, the CuO NPs, which are effectively distributed over the LDH and their synergistic impact in quick dye adsorption followed by rapid photodegradation are attributed to the photocatalytic improvement of the CuO/MgAl-LDHs nanocomposites. It should be highlighted that the strong interaction with LDH aided charge transport and improved the photocatalytic function of composites. The possible degradation mechanism is depicted in Fig. 9.

Conclusions

The CuO semiconductor catalyst synthesized with a green method was combined with MgAl-LDH and applied for the degradation of MB dye. The catalytic performance of the CuO/MgAl-LDHs (1:2) composite exhibited the highest catalytic performance and degraded 99.20% MB dye within 80 min. However, only 90.03, 85.30, 71.87, and 35.53% of MB dye degradation was achieved by CuO/MgAl-LDHs (1:1), CuO/MgAl-LDHs (2:1), CuO NPs, and MgAl-LDHs catalysts, respectively. The enhanced photocatalytic activity was attributed to a synergistic effect, homogeneous dispersion of CuO NPs, adsorption of MB on MgAl-hydroxyl-rich LDH's structure, and lower band gap of CuO NPs. The catalyst stability was also checked and 92.7% of the MB dye removal efficiency was still maintained after five cycles. Therefore, the CuO/MgAl-LDHs-based photocatalyst could be a potential candidate for the environmental remediation.

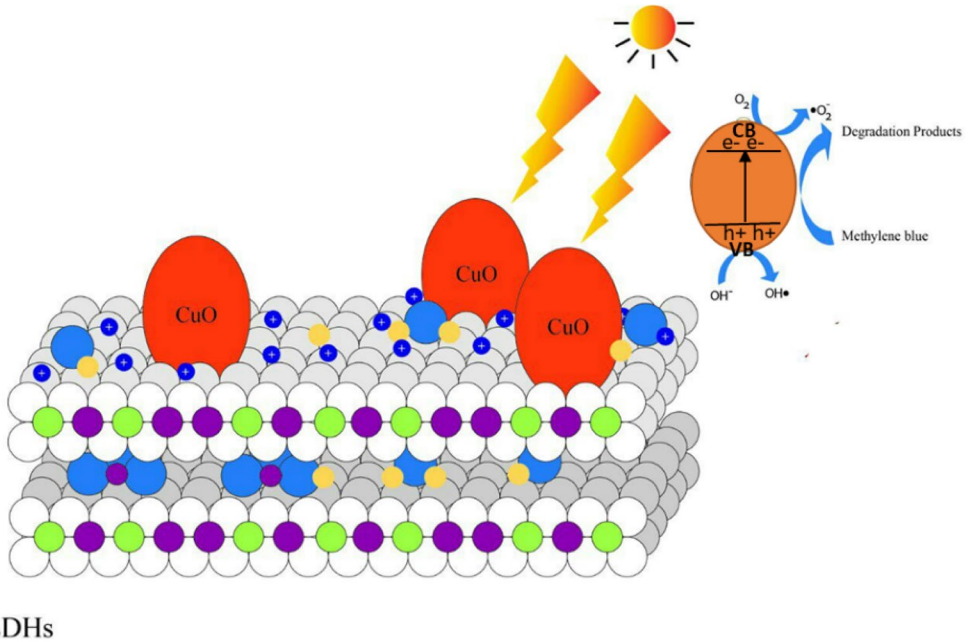

Figure 9. The proposed photocatalytic degradation mechanism of MB with CuO/MgAl-LDHs composites catalyst.

Data availability

All data generated or analyzed during this study are included in this published article.

Received: 5 October 2023; Accepted: 19 January 2024
Published online: 28 January 2024

References

1. Zelekew, O. A., Haitosa, H. H., Chen, X. & Wu, Y.-N. Recent progress on plant extract-mediated biosynthesis of ZnO-based nanocatalysts for environmental remediation: Challenges and future outlooks. *Adv. Colloid Interface Sci.* **317**, 102931 (2023).
2. Daud, M. *et al.* A review on the recent advances, challenges and future aspect of layered double hydroxides (LDH)—Containing hybrids as promising adsorbents for dyes removal. *J. Mol. Liq.* **288**, 110989 (2019).
3. Sun, H. *et al.* A noble bimetal oxysulfide Cu V OS catalyst for highly efficient catalytic reduction of 4-nitrophenol and organic dyes. *RSC Adv.* **9**, 31828–31839 (2019).
4. Manjari, G., Saran, S., Arun, T., Rao, A. V. B. & Devipriya, S. P. Catalytic and recyclability properties of phytogenic copper oxide nanoparticles derived from *Aglaia elaeagnoidea* flower extract. *J. Saudi Chem. Soc.* **21**, 610–618 (2017).
5. Zelekew, O. A. & Kuo, D.-H. Synthesis of a hierarchical structured NiO/NiS composite catalyst for reduction of 4-nitrophenol and organic dyes. *RSC Adv.* **7**, 4353–4362 (2017).
6. Druzian, D. M. *et al.* Cerium oxide nanoparticles: Biosynthesis, characterization, antimicrobial, ecotoxicity and photocatalytic activity. *J. Photochem. Photobiol. A* **442**, 114773 (2023).
7. Moro Druzian, D. *et al.* Cerium oxide nanoparticles: Biosynthesis, characterization, antimicrobial, ecotoxicity and photocatalytic activity. *J. Photochem. Photobiol. A* **442**, 114773 (2023).
8. Muthuvel, A., Jothibas, M. & Manoharan, C. Synthesis of copper oxide nanoparticles by chemical and biogenic methods: Photocatalytic degradation and in vitro antioxidant activity. *Nanotechnol. Environ. Eng.* **5**, 1–19 (2020).
9. Wouters, R. D. *et al.* Zinc oxide nanoparticles: Biosynthesis, characterization, biological activity and photocatalytic degradation for tartrazine yellow dye. *J. Mol. Liq.* **371**, 121090 (2023).
10. Fendrich, M. A., Quaranta, A., Orlandi, M., Bettonte, M. & Miotello, A. Solar concentration for wastewaters remediation: A review of materials and technologies. *Appl. Sci.* **9**, 118 (2018).
11. Varnagiris, S. *et al.* Floating TiO_2 photocatalyst for efficient inactivation of *E. coli* and decomposition of methylene blue solution. *Sci. Total Environ.* **720**, 137600 (2020).
12. Sanakousar, F., Vidyasagar, C., Jiménez-Pérez, V. & Prakash, K. Recent progress on visible-light-driven metal and non-metal doped ZnO nanostructures for photocatalytic degradation of organic pollutants. *Mater. Sci. Semicond. Process.* **140**, 106390 (2022).
13. Abhilash, M. R., Akshatha, G. & Srikantaswamy, S. Photocatalytic dye degradation and biological activities of the Fe_2O_3/Cu_2O nanocomposite. *RSC Adv.* **9**, 8557–8568 (2019).
14. BôlladeMenezes, L. *et al.* Calcium oxide nanoparticles: Biosynthesis, characterization and photocatalytic activity for application in yellow tartrazine dye removal. *J. Photochem. Photobiol. A Chem.* **447**, 115182 (2024).
15. Alsamhary, K., Al-Enazi, N. M., Alhomaidi, E. & Alwakeel, S. Spirulina platensis mediated biosynthesis of CuO Nps and photocatalytic degradation of toxic azo dye Congo red and kinetic studies. *Environ. Res.* **207**, 112172 (2022).
16. Gu, H., Chen, X., Chen, F., Zhou, X. & Parsaee, Z. Ultrasound-assisted biosynthesis of CuO-NPs using brown alga *Cystoseira trinodis*: Characterization, photocatalytic AOP, DPPH scavenging and antibacterial investigations. *Ultrason. Sonochem.* **41**, 109–119 (2018).
17. Hossain, S. S. *et al.* Facile synthesis of CuO/CdS heterostructure photocatalyst for the effective degradation of dye under visible light. *Environ. Res.* **188**, 109803 (2020).
18. Rao, M. P., Wu, J. J., Asiri, A. M., Anandan, S. & Ashokkumar, M. Photocatalytic properties of hierarchical CuO nanosheets synthesized by a solution phase method. *J. Environ. Sci.* **69**, 115–124 (2018).
19. Bordbar, M., Sharifi-Zarchi, Z. & Khodadadi, B. Green synthesis of copper oxide nanoparticles/clinoptilolite using *Rheum palmatum* L. root extract: High catalytic activity for reduction of 4-nitro phenol, rhodamine B, and methylene blue. *J. Sol-Gel Sci. Technol.* **81**, 724–733 (2017).
20. Rafique, M. *et al.* Eco-friendly green and biosynthesis of copper oxide nanoparticles using *Citrofortunella microcarpa* leaves extract for efficient photocatalytic degradation of Rhodamin B dye form textile wastewater. *Optik* **208**, 164053 (2020).
21. Vaidehi, D., Bhuvaneshwari, V., Bharathi, D. & Sheetal, B. P. Antibacterial and photocatalytic activity of copper oxide nanoparticles synthesized using *Solanum lycopersicum* leaf extract. *Mater. Res. Express* **5**, 085403 (2018).
22. Sathiyavimal, S. *et al.* Green chemistry route of biosynthesized copper oxide nanoparticles using *Psidium guajava* leaf extract and their antibacterial activity and effective removal of industrial dyes. *J. Environ. Chem. Eng.* **9**, 105033 (2021).
23. Chia, P. W., Lim, B. S., Tan, K. C., Yong, F. S. J. & Kan, S.-Y. Water extract of onion peel for the synthesis of bisindolylmethanes. *J. King Saud Univ. Sci.* **31**, 642–647 (2019).
24. Dasineh Khiavi, N. *et al.* Visible light driven heterojunction photocatalyst of $CuO–Cu_2O$ thin films for photocatalytic degradation of organic pollutants. *Nanomaterials* **9**, 1011 (2019).
25. Islam, M. R., Saiduzzaman, M., Nishat, S. S., Kabir, A. & Farhad, S. Synthesis, characterization and visible light-responsive photocatalysis properties of Ce doped CuO nanoparticles: A combined experimental and DFT+ U study. *Colloids Surf. A Physicochem. Eng. Asp.* **617**, 126386 (2021).
26. Senobari, S. & Nezamzadeh-Ejhieh, A. A comprehensive study on the enhanced photocatalytic activity of CuO–NiO nanoparticles: Designing the experiments. *J. Mol. Liq.* **261**, 208–217 (2018).
27. Soori, F. & Nezamzadeh-Ejhieh, A. Synergistic effects of copper oxide-zeolite nanoparticles composite on photocatalytic degradation of 2, 6-dimethylphenol aqueous solution. *J. Mol. Liq.* **255**, 250–256 (2018).
28. Khan, I., Khan, I., Usman, M., Imran, M. & Saeed, K. Nanoclay-mediated photocatalytic activity enhancement of copper oxide nanoparticles for enhanced methyl orange photodegradation. *J. Mater. Sci. Mater. Electron.* **31**, 8971–8985 (2020).
29. Ganesan, K. *et al.* Green synthesis of copper oxide nanoparticles decorated with graphene oxide for anticancer activity and catalytic applications. *Arab. J. Chem.* **13**, 6802–6814 (2020).
30. Sapkota, K. P. *et al.* Enhanced visible-light photocatalysis of nanocomposites of copper oxide and single-walled carbon nanotubes for the degradation of methylene blue. *Catalysts* **10**, 297 (2020).
31. Le Hoang, T. T. T., Insin, N. & Sukpirom, N. Catalytic activity of silver nanoparticles anchored on layered double hydroxides and hydroxyapatite. *Inorg. Chem. Commun.* **121**, 108199 (2020).
32. Ma, J. *et al.* In situ reduction for synthesis of nano-sized Cu_2O particles on MgCuAl-LDH layers for degradation of orange II under visible light. *Ceram. Int.* **41**, 3191–3196 (2015).
33. Zhao, G. *et al.* Enhanced photocatalytic degradation of rhodamine B, methylene blue and 4-nitrophenol under visible light irradiation using TiO_2/MgZnAl layered double hydroxide. *J. Mater. Sci. Mater. Electron.* **29**, 7002–7014 (2018).
34. Wang, L. *et al.* TiO_2@ MgAl-layered double hydroxide with enhanced photocatalytic activity towards degradation of gaseous toluene. *J. Photochem. Photobiol. A Chem.* **369**, 44–53 (2019).

35. Zheng, G. *et al.* Facile synthesis of few-layer MoS_2 in MgAl-LDH layers for enhanced visible-light photocatalytic activity. *RSC Adv.* **9**, 24280–24290 (2019).
36. Seftel, E., Mertens, M. & Cool, P. The influence of the Ti4+ location on the formation of self-assembled nanocomposite systems based on TiO_2 and Mg/Al-LDHs with photocatalytic properties. *Appl. Catal. B Environ.* **134**, 274–285 (2013).
37. Dvininov, E., Ignat, M., Barvinschi, P., Smithers, M. & Popovici, E. New SnO_2/MgAl-layered double hydroxide composites as photocatalysts for cationic dyes bleaching. *J. Hazard. Mater.* **177**, 150–158 (2010).
38. Valente, J. S., Tzompantzi, F. & Prince, J. Highly efficient photocatalytic elimination of phenol and chlorinated phenols by CeO_2/MgAl layered double hydroxides. *Appl. Catal. B Environ.* **102**, 276–285 (2011).
39. Wang, Y. *et al.* Silicate silver/flower-like magnalium hydroxide composites for enhanced visible light photodegradation activities. *RSC Adv.* **8**, 23442–23450 (2018).
40. Krishnasamy Sekar, R., Sridhar, A., Perumalsamy, B., Manikandan, D. B. & Ramasamy, T. In vitro antioxidant, antipathogenicity and cytotoxicity effect of silver nanoparticles fabricated by onion (*Allium cepa* L.) peel extract. *BioNanoScience* **10**, 235–248 (2020).
41. Nayak, S. & Parida, K. Nanostructured CeO_2/MgAl-LDH composite for visible light induced water reduction reaction. *Int. J. Hydrog. Energy* **41**, 21166–21180 (2016).
42. Shan, R.-R. *et al.* Magnetic Fe_3O_4/MgAl-LDH composite for effective removal of three red dyes from aqueous solution. *Chem. Eng. J.* **252**, 38–46 (2014).
43. Kokilavani, S. *et al.* Enhanced visible light driven photocatalytic and antibacterial activities of Ag_2WO_4 decorated ZnS nanocomposite. *Ceram. Int.* **47**, 12997–13006 (2021).
44. Yang, Y. *et al.* Urchin-like hierarchical CoZnAl-LDH/RGO/g-C_3N_4 hybrid as a Z-scheme photocatalyst for efficient and selective CO_2 reduction. *Appl. Catal. B Environ.* **255**, 117771 (2019).
45. Haitosa, H. H. *et al.* Stephania abyssinica leaf extract mediated (Mn, Ni) co-doped ZnO catalyst synthesis for the degradation of organic dye. *J. Mol. Liq.* **368**, 120666 (2022).
46. Patel, M., Mishra, S., Verma, R. & Shikha, D. Synthesis of ZnO and CuO nanoparticles via Sol gel method and its characterization by using various technique. *Discov. Mater.* **2**, 1 (2022).
47. Druzian, D. M. *et al.* A bimetallic nanocatalyst from carbonaceous waste for crystal violet degradation. *Mater. Chem. Phys.* **297**, 127455 (2023).
48. Bekru, A. G., Zelekew, O. A., Andoshe, D. M., Sabir, F. K. & Eswaramoorthy, R. Microwave-assisted synthesis of CuO nanoparticles using *Cordia africana* Lam. leaf extract for 4-nitrophenol reduction. *J. Nanotechnol.* **2021**, 5581621 (2021).
49. Li, Z., Chen, M., Ai, Z., Wu, L. & Zhang, Q. Mechanochemical synthesis of CdS/MgAl LDH-precursor as improved visible-light driven photocatalyst for organic dye. *Appl. Clay Sci.* **163**, 265–272 (2018).
50. Naseem, S., Gevers, B. R., Labuschagné, F. J. & Leuteritz, A. Preparation of photoactive transition-metal layered double hydroxides (LDH) to replace dye-sensitized materials in solar cells. *Materials* **13**, 4384 (2020).
51. Yuan, J. *et al.* CuO nanoparticles supported on TiO_2 with high efficiency for CO_2 electrochemical reduction to ethanol. *Catalysts* **8**, 171 (2018).
52. Zhou, Z., Lu, C., Wu, X. & Zhang, X. Cellulose nanocrystals as a novel support for CuO nanoparticles catalysts: Facile synthesis and their application to 4-nitrophenol reduction. *RSC Adv.* **3**, 26066–26073 (2013).
53. Choi, J. *et al.* Preparation and characterization of graphene oxide supported Cu, Cu_2O, and CuO nanocomposites and their high photocatalytic activity for organic dye molecule. *Curr. Appl. Phys.* **17**, 137–145 (2017).
54. Chen, J. *et al.* Engineering ultrafine NiS cocatalysts as active sites to boost photocatalytic hydrogen production of MgAl layered double hydroxide. *Appl. Surf. Sci.* **506**, 144999 (2020).
55. Bhuvaneswari, K., Palanisamy, G., Pazhanivel, T., Bharathi, G. & Nataraj, D. Photocatalytic performance on visible light induced ZnS QDs-MgAl layered double hydroxides hybrids for methylene blue dye degradation. *ChemistrySelect* **3**, 13419–13426 (2018).
56. Zhen, S.-Y. *et al.* Metal–organic framework derived hollow porous CuO–$CuCo_2O_4$ dodecahedrons as a cathode catalyst for Li–O_2 batteries. *RSC Adv.* **9**, 16288–16295 (2019).
57. Veisi, H. *et al.* Biosynthesis of CuO nanoparticles using aqueous extract of herbal tea (*Stachys lavandulifolia*) flowers and evaluation of its catalytic activity. *Sci. Rep.* **11**, 1–13 (2021).
58. de Menezes, L. B. *et al.* Calcium oxide nanoparticles: Biosynthesis, characterization and photocatalytic activity for application in yellow tartrazine dye removal. *J. Photochem. Photobiol. A Chem.* **447**, 115182 (2024).
59. Mobarak, M. B., Hossain, M. S., Chowdhury, F. & Ahmed, S. Synthesis and characterization of CuO nanoparticles utilizing waste fish scale and exploitation of XRD peak profile analysis for approximating the structural parameters. *Arab. J. Chem.* **15**, 104117 (2022).
60. Shnoudeh, A. J. *et al.* In *Biomaterials and Bionanotechnology* (ed. Tekade, R. K.) 527–612 (Academic Press, 2019).
61. Lem, O., Yoon, S., Bae, S. & Lee, W. The enhanced reduction of bromate by highly reactive and dispersive green nano-zerovalent iron (G-NZVI) synthesized with onion peel extract. *RSC Adv.* **11**, 5008–5018 (2021).
62. Li, X. *et al.* Synthesis of MgAl LDH/Acidified g-C3N4 heterojunction photocatalyst for improved tetracycline hydrochloride degradation activity. *Nano* **14**, 1950066 (2019).
63. Kerchich, S., Boudjemaa, A., Chebout, R., Bachari, K. & Mameri, N. High performance of δ-Fe_2O_3 novel photo-catalyst supported on LDH structure. *J. Photochem. Photobiol. A Chem.* **406**, 113001 (2021).
64. Ni, J. *et al.* Construction of magnetically separable NiAl LDH/Fe_3O_4–RGO nanocomposites with enhanced photocatalytic performance under visible light. *Phys. Chem. Chem. Phys.* **20**, 414–421 (2018).
65. Zhou, Y., Hu, W., Yu, J. & Jiao, F. Effective photocatalytic degradation of methylene blue by Cu_2O/MgAl layered double hydroxides. *React. Kinet. Mech. Catal.* **115**, 581–596 (2015).
66. Fu, S., Zheng, Y., Zhou, X., Ni, Z. & Xia, S. Visible light promoted degradation of gaseous volatile organic compounds catalyzed by Au supported layered double hydroxides: Influencing factors, kinetics and mechanism. *J. Hazard. Mater.* **363**, 41–54 (2019).
67. George, A. *et al.* Photocatalytic effect of CuO nanoparticles flower-like 3D nanostructures under visible light irradiation with the degradation of methylene blue (MB) dye for environmental application. *Environ. Res.* **203**, 111880 (2022).
68. Zelekew, O. A., Kuo, D.-H., Yassin, J. M., Ahmed, K. E. & Abdullah, H. Synthesis of efficient silica supported TiO_2/Ag_2O heterostructured catalyst with enhanced photocatalytic performance. *Appl. Surf. Sci.* **410**, 454–463 (2017).
69. Chen, X. *et al.* Synthesis of visible light responsive iodine-doped mesoporous TiO_2 by using biological renewable lignin as template for degradation of toxic organic pollutants. *Appl. Catal. B Environ.* **252**, 152–163 (2019).

Acknowledgements

This M.Sc. thesis was funded by Adama Science and Technology University under the grant number of ASTU/SM-R/608/22, Adama, Ethiopia. We also acknowledged National Taiwan University of Science and Technology, Department of Materials Science and Engineering for SEM/EDS, TEM, and XPS analysis.

Author contributions

H.T.B.: Investigation; Writing—Original Draft. D.M.A.: Writing—Review and Editing. N.S.G.: Characterization; Writing—Review and Editing. D.-H.K.: Writing—Review and Editing. X.C.: Writing—Review and Editing. H.A.:

Writing—Review and Editing. T.H.W.: Writing—Review and Editing. Y.W.: Writing—Review and Editing. O.A.Z.: Supervision, Resources; Conceptualization; Writing—Review and Editing.

Competing interests
The authors declare no competing interests.

Additional information
Supplementary Information The online version contains supplementary material available at https://doi.org/10.1038/s41598-024-52547-w.

Correspondence and requests for materials should be addressed to O.A.Z.

Reprints and permissions information is available at www.nature.com/reprints.

Publisher's note Springer Nature remains neutral with regard to jurisdictional claims in published maps and institutional affiliations.